Solitonlike propagation in photorefractive crystals with large optical activity and absorption

E. Fazio
Università degli Studi di Roma "La Sapienza" and INFM Dipartimento di Energetica, via Scarpa 16, I-00161 Roma, Italy

V. Babin
Institute of Atomic Physics, NIOE Atomistii 111, R-76900 Bucharest, Romania

M. Bertolotti
Università degli Studi di Roma "La Sapienza" and INFM Dipartimento di Energetica, via Scarpa 16, I-00161 Roma, Italy

V. Vlad
Institute of Atomic Physics, NILPRP-Department of Lasers and The Romanian Academy-CASP Atomistii 111, R-76900 Bucharest, Romania

(Received 27 December 2001; published 22 July 2002)

We have found analytical solutions of the light propagation equations in photorefractive materials with strong optical activity and absorption. These solutions show the occurrence of breathing solitons in sillenite crystals with strong optical activity and absorption in two particular orientations with respect to the external electric field. The absorption is decreasing the soliton intensity with the propagation distance (which set a limit in the soliton channel length), is increasing the breathing period, and is changing the soliton width (in inverse relations, at low and high intensities). Our experimental results confirm the analytical solutions and the numerical simulations, as well as the importance of the optical activity and absorption in solitonlike propagation.

DOI: 10.1103/PhysRevE.66.016605 PACS number(s): 42.65.Tg, 42.65.Jx, 42.65.Hw

I. INTRODUCTION

Steady-state spatial solitons at low laser intensity have been proved to exist by $(1+1)$D and $(2+1)$D (D means dimensional) compensation of diffraction by refractive index modulation in photorefractive crystals [1–11].

The steady-state (screening) solitons were first predicted by Segev *et al.* [1,2] and by Christodoulidis and Carvalho [3]. They assumed the (incoherent) superimposition of the focused signal beam on a collimated background beam into a photorefractive crystal (PRC). The background ensures a constant pumping of electric charges, provides the dependence of the refractive index change on the average light intensity in steady-state conditions, and drives the system to a stable modification of the refractive index, i.e., to a stable soliton formation in the signal beam propagation. In order to obtain the spatial soliton, both beams are propagating parallel along an appropriate crystallographic axis of the photorefractive crystal and perpendicular to an external electric field, which creates a dominant drift regime for the photorefractive effects. The static electric field inside the crystal is decreased (screened) in the region of the focused beam, with a narrow Gaussian spatial distribution and a high optical intensity in the center. The resulting electric space-charge field induces a spatial refractive index modulation in the form of a waveguide, which preserves the solitonic shape of the propagating signal beam. The theory of steady-state solitons in PRC was further developed by Crosignani *et al.* [4,5].

Experimental observation of $(2+1)$D and $(1+1)$D steady-state solitons and self-focusing in PRC was done by Shih *et al.* [6,9], Iturbe Castillo *et al.* [7,8], Kos *et al.* [10], Chen *et al.* [11], Fressengeas *et al.* [12], Wolfensberger *et al.* [13]. Segev *et al.* [14] and Crosignani *et al.* [15] wrote good reviews over the major achievements in the field. Soliton interaction is being largely investigated too, see, for example, the review by Denz *et al.* [16].

Many photorefractive crystals (for example, the sillenites) and organic nonlinear materials show important optical activity [17], which complicates the wave propagation in these anisotropic nonlinear media. Singh and Christodoulidis [18] and Krolikowski *et al.* [19] developed theoretical models and numerical calculations for studying wave propagation and possible $(1+1)$D soliton formation in these complex media. They have shown that for some crystallographic orientations and properly chosen beam intensity, nearly stationary propagation of solitonlike waves is possible. We have obtained analytical and numerical results within a theoretical model for $(2+1)$D solitonic propagation in photorefractive crystals with strong optical activity [20,21] and experimental results proving the generation of $(1+1)$D solitons in $Bi_{12}SiO_{20}$ (BSO) crystals, at high external electric fields [21]. In this paper, we describe $(2+1)$D analytical solutions of propagation equations in PRC with strong optical activity and absorption. The relatively large absorption was previously [22–24] correlated with good photorefractive properties and consequently, it cannot be neglected in a realistic treatment of spatial solitons. The existence of $(2+1)$D "breathing" solitons (solitonlike waves) is demonstrated for particular orientations of the crystals belonging to the sillenite family. The dependence of the soliton features on different controllable parameters is also derived. Experimental results, as well as numerical simulations in BSO crystals, confirm these analytical solutions and the importance of optical activity and absorption in soliton formation.

II. LIGHT PROPAGATION IN PHOTOREFRACTIVE CRYSTALS WITH INDUCED BIREFRINGENCE, OPTICAL ACTIVITY, AND ABSORBTION

The light propagation in a nonlinear anisotropic material with optical activity and absorption can be described by the wave equation for the electric vector of the optical field [10,11]:

$$\nabla^2\vec{E}(\vec{r},t)-\frac{1}{c^2}\left[\hat{\varepsilon}\otimes\frac{\partial^2\vec{E}}{\partial t^2}+\frac{g}{k}\left(\vec{\nabla}\times\frac{\partial^2\vec{E}}{\partial t^2}\right)\right]-\frac{n_0}{c}\alpha\frac{\partial\vec{E}}{\partial t}=0, \tag{1}$$

where c is the light velocity in vacuum, $\hat{\varepsilon}$ is the symmetric dielectric permittivity tensor of the anisotropic material, "$\otimes$" is the tensor-vector multiplication, $g=2\rho_0/k$ is the gyration constant, ρ_0 is the optical rotating power, n_0 the refractive index, α the absorption, and k is the wave vector inside the material.

Considering the classical solution of the form

$$\vec{E}(\vec{r},t)=\vec{A}(\vec{r})e^{i(ks-\omega t)} \tag{2}$$

and introducing the slowly varying envelope approximation (SVEA), Eq. (1) becomes

$$2ik\frac{\partial\vec{A}}{\partial z}+\frac{\partial^2\vec{A}}{\partial x^2}+\frac{\partial^2\vec{A}}{\partial y^2}-k^2\vec{A}+k^2\hat{\varepsilon}\otimes\vec{A}+ik^2g(\vec{e}_z\times\vec{A})$$

$$+k^2\frac{g}{k}(\vec{\nabla}\times\vec{A})+ik\alpha\vec{A}=0. \tag{3}$$

In a simplified single species model, the photorefractive effect consists of the photoionization of some donors and the refractive index modulation by the resulting electric space-charge field (including carrier transport and recombination). In the steady-state and drift dominated transport conditions, the change of the dielectric permittivity tensor as a function of light intensity is described by a simple equation [2–4,10,11]. Crosignani *et al.* [4] found out that, in both (1+1)D and (2+1)D cases, the dependence of the dielectric permittivity tensor on the optical field intensity is given in a good approximation by

$$\hat{\varepsilon}=[\vec{E}_0\hat{R}n_0^2][1+(\vec{A}/\sqrt{I_B})^2]^{-1}+\hat{\varepsilon}_0,\quad \hat{\varepsilon}_0=\begin{bmatrix}\varepsilon_{xx} & 0\\ 0 & \varepsilon_{yy}\end{bmatrix}, \tag{4}$$

where E_0 is the external electric field applied perpendicularly to the optical beams, along the *OX* axis, $\hat{R}$ is the electro-optic tensor of the anisotropic material, I_B is the background intensity, and ε_0 is the dielectric permittivity tensor in the dark (Fig. 1).

For a dispersionless optical activity we can write $\vec{\nabla}\times\vec{A}=\vec{0}$ (as justified in [17]). In this case Eq. (3) can be written in a more compact form using a new field, $\vec{B}=-\vec{M}\times\vec{A}=-m\hat{e}_z\times\vec{A}$, where $\vec{M}=m\hat{e}_z$ is the angular momentum of the soliton beam and $\hat{e}_z$ represents the unitary vector along the propagation z axis. Thus a vanishing curl of A means that the angular momentum of the solitonic beam m is a constant of motion. If the curl of A does not vanish, the optical activity acts as a friction for the polarization rotation, destroying the soliton that no longer conserves its angular momentum. This condition, i.e., a constant angular momentum of the soliton, has been confirmed experimentally too.

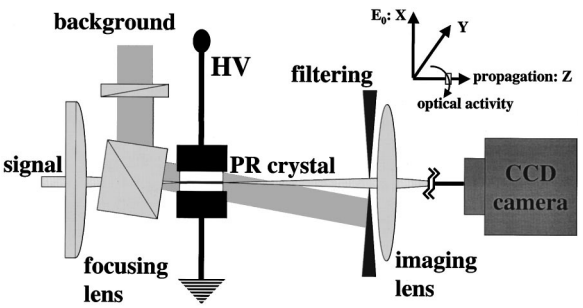

FIG. 1. Wave propagation configuration in a photorefractive crystal for screening spatial soliton formation.

Using the normalized variables, $\xi=kx$; $\eta=ky$; $\zeta=kz$, Eq. (3) becomes

$$\hat{L}\begin{bmatrix}B_x\\ B_y\end{bmatrix}+\begin{bmatrix}(\varepsilon_{yy}-1) & (\varepsilon_{xy}+ig_1)\\ (\varepsilon_{xy}-ig_1) & (\varepsilon_{xx}-1)\end{bmatrix}\begin{bmatrix}B_x\\ B_y\end{bmatrix}=0. \tag{5}$$

In Eq. (5), we have introduced the operator

$$\hat{L}=2i\frac{\partial}{\partial\zeta}+\frac{\partial^2}{\partial\xi^2}+\frac{\partial^2}{\partial\eta^2}$$

and the effective gyration constant, $g_1=2[\rho_0-(\alpha/2)]/k$, which includes the effects of the linear optical absorption. One can diagonalize the permittivity tensor from Eq. (5) by a counterclockwise rotation of the plane (B_x,B_y) by the angle $\varphi'=\frac{1}{2}\arctan g[2\varepsilon_{xy}/(\varepsilon_{xx}-\varepsilon_{yy})]$, which leads to new field components (B_x',B_y').

For cubic PRC and for the coincidence of the optical field axis (z axis) with one of the principal directions of the index ellipsoid, one finds

$$\varepsilon_{xx}=\varepsilon_{yy}=1,\quad \varepsilon_{xy}=\frac{c_1}{1+(B_x'^2+B_y'^2)/I_B},$$

$$c_1=n_0^2r_{41}E_0=(1/n_0^2)\Delta n\rightarrow\varphi'=\pi/4, \tag{6}$$

with Δn being the refractive index change due to the photorefractive effect (induced birefringence).

Introducing the normalized field components, $u=B_x'/\sqrt{I_B}$, $v=B_y'/\sqrt{I_B}$, Eq. (5) takes the form

$$\hat{L}\begin{bmatrix}u\\ v\end{bmatrix}+\begin{bmatrix}(1+u^2+v^2)^{-1} & -ig_1/c_1\\ +ig_1/c_1 & \mu(1+u^2+v^2)^{-1}\end{bmatrix}\begin{bmatrix}u\\ v\end{bmatrix}=0, \tag{7}$$

where μ takes the values 0 or -1 for the two important orientations of the crystal, with the electric field along the [001] and [110] directions, respectively. The rotation of the light electric vector by the optical activity is more conve-

niently described by the *wave equation in cylindrical coordinates* (*scaled to the nonlinear birefringence coefficient*, c_1):

$$\xi' = \rho\cos\varphi, \quad \eta' = \rho\sin\varphi, \quad \zeta' = \zeta = c_1 kz,$$

$$\rho = \sqrt{\xi'^2 + \eta'^2} = \sqrt{c_1}k\sqrt{x^2+y^2}, \quad \varphi = \arctan(y/x).$$

Moreover, the separation of the slow components (envelopes u_1, v_1) from the fast ones (φ) in the field vector, as

$$\begin{vmatrix} u(\rho,\varphi,\zeta') \\ v(\rho,\varphi,\zeta') \end{vmatrix} = \sqrt{2/\pi}\,\frac{\sin^2(\rho+\rho_0')}{\sqrt{\rho+\rho_0'}} \begin{bmatrix} \cos(\varphi/2) & \sin(\varphi/2) \\ -\sin(\varphi/2) & \cos(\varphi/2) \end{bmatrix} \times \begin{bmatrix} u_1(\rho,\zeta') \\ v_1(\rho,\zeta') \end{bmatrix} \tag{8}$$

transforms Eq. (7) into

$$2i\frac{\partial\vec{u}}{\partial\zeta'} + \frac{\partial^2\vec{u}}{\partial\rho^2} + \begin{bmatrix} (1+u^2+v^2)^{-1} & 0 \\ 0 & \mu(1+u^2+v^2)^{-1} \end{bmatrix} \begin{bmatrix} u_1 \\ v_1 \end{bmatrix} + i(g_1/c_1)(\vec{e}_2\times\vec{u}) = 0. \tag{9}$$

In Eq. (8), $\rho_0' = \pi/2$ is the integration constant for the slow component. The width of the main lobe of the factor $\sin^2(\rho+\rho_0')/\sqrt{\rho+\rho_0'}$, which appears in the field envelope, is expected to be much larger than the soliton width and consequently we shall approximate this factor by 1.

In order to separate the induced birefringence and the optical activity, we can take the envelope vector to rotate in the reference frame of the optical activity by the angle $g_1\zeta'/c_1 = g_1 kz$, i.e., to transform it into a new vector $\vec{\Phi}(\rho,\zeta')$ by the vectorial product with an axial vector $\vec{\gamma}(\varphi,\zeta')$,

$$\vec{u} = \begin{vmatrix} u_1 \\ v_1 \end{vmatrix} = \vec{\Phi}(\rho,\zeta')\times\vec{\gamma}(\varphi,\zeta'). \tag{10}$$

We can restrict the form of the axial vector $\vec{\gamma}(\varphi,\zeta')$ by the condition

$$2i\vec{\Phi}\times\frac{\partial\vec{\gamma}}{\partial\zeta'} + i\delta[\vec{e}_z\times(\vec{\Phi}\times\vec{\gamma})] = 0, \tag{11}$$

which eliminates the rotating term from Eq. (9) and leads to the solution [17]

$$\gamma(\varphi,\zeta') \approx e^{-\alpha z/2}|\cos\theta|^2, \tag{12}$$

with $\theta = \frac{1}{2}[\varphi - 2\varphi' + (g_1/c_1)\zeta' - 2\zeta_0'] = (1/2)[\varphi + g_1 kz - (\pi/2)]$.

In Eq. (12), we can take $\varphi' = \pi/4$ for cubic crystals and the initial phase of the optical activity $\zeta_0' = 0$ from suitable boundary conditions to ensure the continuity with the Gaussian input beam. The axial vector $\gamma(\varphi,\zeta')$ leads to transverse oscillations (breathing) of the propagating wave with the period

$$\lambda_b = 2\lambda/g_1 = 2\pi/[\rho_0 - (\alpha/2)]. \tag{13}$$

When $\cos\theta = 0$, the modulus of this axial vector is singular, but the light field is limited by other factors in the solutions, which compensate this behavior and ensure the power conservation, as will be shown.

After the transformation from Eq. (10) and the use of condition (11), Eq. (9) becomes

$$2i\frac{\partial\vec{\Phi}_1}{\partial\zeta'} + \frac{\partial^2\vec{\Phi}}{\partial\rho^2} + \begin{bmatrix} (1+u^2+v^2)^{-1} & 0 \\ 0 & \mu(1+u^2+v^2)^{-1} \end{bmatrix} \begin{bmatrix} \Phi_{x1} \\ \Phi_{y1} \end{bmatrix} = 0. \tag{14}$$

The transformation of the Φ-vector components back into the amplitude components of the light electric field can be found from

$$\begin{bmatrix} A_x \\ A_y \end{bmatrix} = \sqrt{2I_B r/\pi}\,\gamma(\varphi,\zeta') \begin{bmatrix} \sin\theta & -\cos\theta \\ \cos\theta & \sin\theta \end{bmatrix} \begin{bmatrix} \Phi_{x1} \\ \Phi_{y1} \end{bmatrix}. \tag{15}$$

Within SVEA, one can take

$$u^2 + v^2 = (2/\pi)[\Phi_{x1}^2 + \Phi_{y1}^2]\gamma^2. \tag{16}$$

To proceed further with solving the propagation equations, we shall do some piecewise linearizations of the permittivity (space-charge) characteristic function of the photorefractive crystals.

A. Solitonlike analytical solutions of the wave equations in PRC with optical activity and absorption at low intensity levels

At *low light intensity levels*, the intensity dependent factor from Eq. (4) can be approximated by $(1-I/I_B) = 1 - r(I/I_0)$, (I_0 is the maximum input intensity, $r = I_0/I_B$) and Eqs. (14) become

$$2i\frac{\partial\Phi_{x1}}{\partial\zeta'} + \frac{\partial^2\Phi_{x1}}{\partial\rho^2} + \mu\left[1 - \frac{2r}{\pi}\gamma^2(\varphi,\zeta')(\Phi_{x1}^2+\Phi_{y1}^2)\right]\Phi_{x1} = 0,$$

$$2i\frac{\partial\Phi_{y1}}{\partial\zeta'} + \frac{\partial^2\Phi_{y1}}{\partial\rho^2} + \left[1 - \frac{2r}{\pi}\gamma^2(\varphi,\zeta')(\Phi_{x1}^2+\Phi_{y1}^2)\right]\Phi_{y1} = 0. \tag{17}$$

We are looking for spatial solitons, therefore, we are interested in the transverse component decoupling. This decoupling is based on the large period ratio of the transverse and axial oscillations, which allows us to write the Φ functions as

$$\Phi_{x1} = e^{i\mu\zeta'/2}\psi_x(\rho), \quad \Phi_{y1} = e^{i\zeta'/2}\psi_y(\rho),$$

$$(\psi_x^2 + \psi_y^2) \leqslant |\psi_x|^2 + |\psi_y|^2. \tag{18}$$

The substitution of Eq. (18) into Eqs. (17) leads to the transverse (envelope) equation system

$$\frac{\partial^2\psi_x(\rho)}{\partial\rho^2} - \mu\frac{2r}{\pi}\gamma^2(\varphi,\zeta')(\psi_x^2+\psi_y^2)\psi_x = 0,$$

$$\frac{\partial^2\psi_y(\rho)}{\partial\rho^2}-\frac{2r}{\pi}\gamma^2(\varphi,\zeta')(\psi_x^2+\psi_y^2)\psi_y=0, \tag{19}$$

where the new ψ functions are related to optical (electric) field components by

$$\begin{bmatrix}A_x\\A_y\end{bmatrix}=\sqrt{2I_Br/\pi}\gamma(\varphi,\zeta')\begin{bmatrix}\sin\theta & -\cos\theta\\ \cos\theta & \sin\theta\end{bmatrix}\times\begin{bmatrix}e^{i\mu\zeta'/2} & \psi_x(\rho_1)\\ e^{i\zeta'/2} & \psi_y(\rho_1)\end{bmatrix}. \tag{20}$$

In Eq. (20), we have denoted

$$\rho_1=\sqrt{2r/\pi}\gamma(\varphi,z)\rho=\sqrt{2r/\pi}e^{-\alpha z/2}\left|\cos\left(\frac{1}{2}\right)\times\left(\varphi+g_1kz-\frac{\pi}{2}\right)\right|^{-1}\rho=\rho/(\Delta\rho)_1 \tag{21}$$

and $(\Delta\rho)_1$ is the normalized beam width (for $r\ll1$).

At this point, we shall take into account the two important orientations of the cubic crystals, imposing the above-mentioned particular values for the parameter μ.

Case 1. $\mu=0$ (the external electric field oriented along [001] direction). The solutions of Eqs. (17) and (19) are

$$\psi_x(\rho_1)=\psi_{x0}\exp\{-[\rho_1^2w_0^2/(w_0^4+4\zeta'^2)]\}\times[\pi^2(w_0^4+4\zeta'^2)]^{-1/4},$$

$$\psi_y(\rho_1)=\pm\frac{i\sqrt{2}\psi_x}{\cosh(\psi_{x0}\sqrt{2}\rho_1)}, \tag{22}$$

where ψ_{x0} is the wave amplitude (by normalization, $\psi_{x0}=1$) and w_0 is the input Gaussian beam width. The optical field components are

$$\begin{bmatrix}A_x\\A_y\end{bmatrix}=\sqrt{2I_Br/\pi}\gamma(\varphi,\zeta')\begin{bmatrix}\sin\theta & -\cos\theta\\ \cos\theta & \sin\theta\end{bmatrix}\begin{bmatrix}\exp\{-[\rho_1^2w_0^2/(w_0^4+4\zeta'^2)]\}[\pi^2(w_0^4+4\zeta'^2)]^{-1/4}\\ i\sqrt{2}\cosh^{-1}(\sqrt{2}\rho_1)\exp\{-[\rho_1^2/(w_0^2+4\zeta'^2/w_0^2)]\}[\pi^2(w_0^4+4\zeta'^2)]^{-1/4}\end{bmatrix} \tag{23}$$

defining a wave, which has a confined ''breathing'' core and a weak diffraction part in both components. The total intensity of this wave is

$$I(\rho,\varphi,\zeta')=(2/\pi)I_B(r\gamma^2)[\psi_x^2+\psi_y^2]\approx(2/\pi^2w_0^2)I_B(r\gamma^2)\times\exp(-2\rho_1^2/w_0^2)[1+2\cosh^{-2}(\sqrt{2}\rho_1)]. \tag{24}$$

The approximation holds for short crystals (BSO crystals usually used, due to large absorption). One can remark that the jumps of γ function (when $\cos\theta=0$) are balanced by the exponential factor, so that the total intensity preserves the solitonlike shape. The initial conditions lead to the relation, $w_0\approx6r/\pi^{3/2}$ and to small w_0, which are restrictive conditions for $(2+1)$D solitons.

The total intensity from Eq. (24) can be graphically shown, as a function of the propagation distance, for an optical activity of 10°/mm (in Figs. 2(a, b), as for $Bi_{12}TiO_{20}$ (BTO) crystals [17]) and for an optical activity of 45°/mm (in Fig. 2(c), as for BSO crystals [17]). In these figures, the crystal length is chosen to be 8 mm, the input Gaussian beam width is 10 μm, and $r=0.1$. One can remark that the solitonlike propagation is maintained in the presence of optical activity and absorption with better confinement at higher external electric fields. The increase of optical activity (at given absorption coefficient) decreases the soliton breathing period and the increase of absorption coefficient (at a given optical activity) slightly increases the soliton breathing period with a simultaneous increase of soliton width and attenuation.

The soliton width is obtained by combining the maximum width of the hyperbolic secant (at the maximum values of cos function):

$$(\Delta\rho)_1=\sqrt{\pi/2r}\ \frac{1}{\gamma}=\sqrt{\pi/2r}e^{+\alpha z/2}\left|\left[\cos\left\{z\left(\rho_0-\frac{\alpha}{2}\right)+\frac{\varphi}{2}-\frac{\pi}{4}\right\}\right]\right|, \tag{25a}$$

which is close to a corresponding Gaussian function and the width of the Gaussian function of Eq. (24). Thus, we can calculate the maximum soliton width by

$$(\Delta\rho_t)^{-2}\approx(\Delta\rho_{1\,\max})^{-2}+(\sqrt{\pi}w_0/\gamma\sqrt{r})^{-2}. \tag{25b}$$

We can observe that the soliton maximum width is smaller than the Gaussian input beam (as expected) and decreases also with the increase of the beam ratio, r. All transverse variables were normalized by the factor $k\sqrt{n_0^2r_{41}E_0}=(2\pi n_0^2/\lambda_0)\sqrt{r_{41}E_0}$; thus, one can obtain the soliton maximum width as

$$w_{s\,\max}=(\Delta\rho_t)/k\sqrt{n_0^2r_{41}E_0} \tag{25c}$$

and deduce its decrease when the external electric field is increased.

Case 2. $\mu=-1$ (electric field oriented along [110] direction). Equations (19) become

$$\frac{\partial^2\psi_x}{\partial\rho_1^2}+(\psi_x^2+\psi_y^2)\psi_x=0,$$

$$\frac{\partial^2\psi_y}{\partial\rho_1^2}-(\psi_x^2+\psi_y^2)\psi_y=0. \tag{26}$$

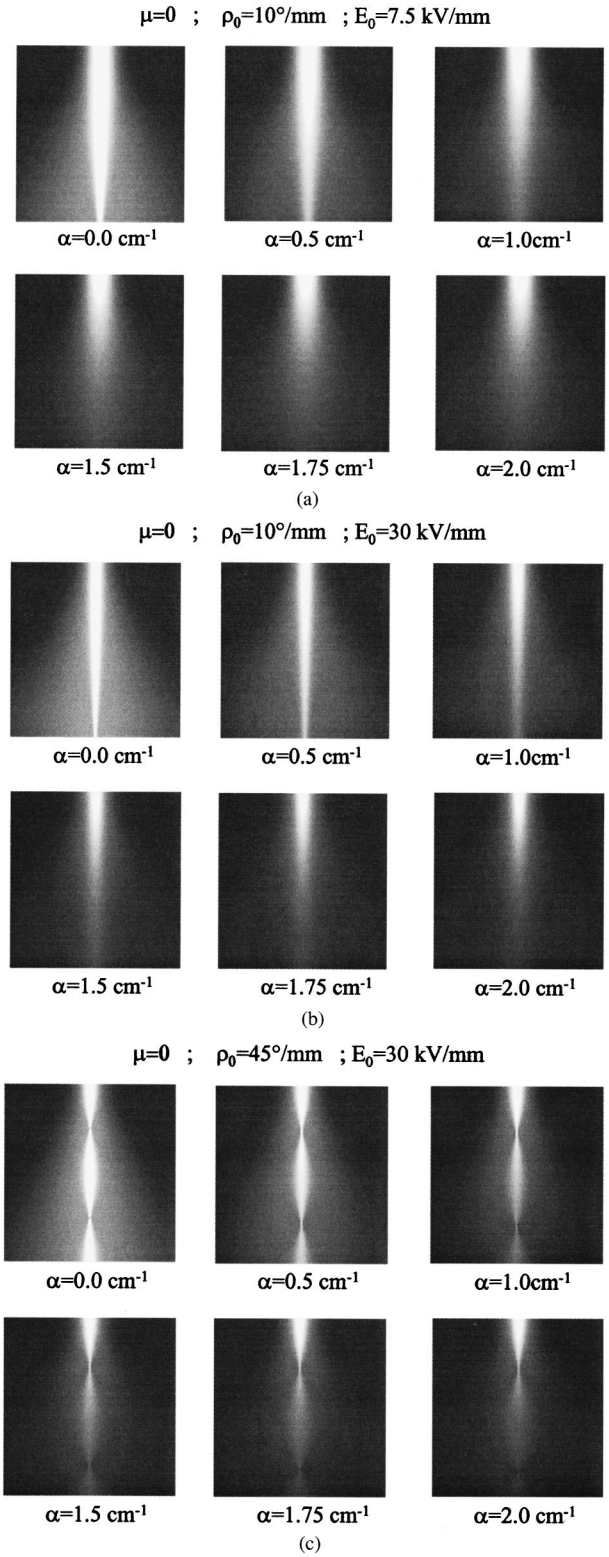

FIG. 2. The total intensity of the propagating wave as a function of the distance with the external electric field, E_0, applied along the [001] crystal direction ($\mu=0$, perpendicular to the vertical propagation axis, Oz), for different absorption coefficients. The maximum propagation distance was taken 8 mm. (a) BTO crystal (optical activity $\rho=10°/\mathrm{mm}$), $E_0=7.5$ kV/mm, (b) BTO crystal, $E_0=30$ kV/mm; (c) BSO crystal (optical activity $\rho=45°/\mathrm{mm}$), $E_0=30$ kV/mm (according to the material parameters in [17]).

Passing through the characteristic equations of the system (26) and a differential equation of Riccati type [17], we found out the solutions at low intensity levels (ψ_{x0}, $\psi_{y0}\ll 1$),

$$\psi_x(\rho_1,z)=(\psi_{x0}/2)\{(4/3)[-\cosh\rho_1+\ln|\tanh(\rho_1/2)|]^{-1}-(\cosh\rho_1)^{-1}\},$$
$$\psi_y(\rho_1,z)=(\psi_{y0}/2)\{(4/3)[-\cosh\rho_1+\ln|\tanh(\rho_1/2)|]^{-1}+(c\cosh\rho_1)^{-1}\}, \tag{27}$$

and the optical field components (for cubic crystals)

$$\begin{bmatrix}A_x\\A_y\end{bmatrix}=\sqrt{2I_B r/\pi}\,\gamma(\varphi,\zeta')\begin{bmatrix}\sin\theta & -\cos\theta\\ \cos\theta & \sin\theta\end{bmatrix}\times\begin{bmatrix}e^{-i\zeta'/2}\psi_x(\rho_1,z)\\ e^{i\zeta'/2}\psi_y(\rho_1,z)\end{bmatrix}, \tag{28}$$

which is *a breathing solitonlike wave* along both axes. Considering the initial conditions (the identity with the 2D symmetrical Gaussian input beam), $\psi_{x0}=\psi_{y0}=\psi_0=(2\sqrt{\pi}/w_0)^{1/2}$, the soliton like beam intensity is

$$I=A_x^2+A_y^2=\frac{1}{\sqrt{\pi}w_0}I_B r\,\gamma^2(\varphi,\zeta')\times\left\{\frac{\frac{16}{9}}{\left[\ln\left(\left|\tanh\left(\frac{\rho_1}{2}\right)\right|\right)-\cosh\rho\right]^2}+\frac{1}{(\cosh\rho_1)^2}\right\}. \tag{29}$$

One can remark that, for this crystal orientation, the *y* component is a transversely modulated (breathing) soliton and the *x* component is a deformed version of the former one due to the logarithmic term. The same initial conditions lead to a relation between the input beam width and the beam ratio, *r*, namely: $w_0^2=\pi/2r$, which confirms the restrictive conditions for $(2+1)$D solitons observed in experiments with other materials. The total intensity of this breathing soliton can be graphically represented, for BTO [Figs. 3(a, b)] and BSO [Fig. 3(c)] crystals, respectively, as a function of the propagation distance.

The solitonic channel produced by Eq. (29) is

$$(\Delta\rho)_1\approx\sqrt{\pi/2r}\frac{1}{\gamma}=\sqrt{\pi/2r}\,e^{+\alpha z/2}\left|\left[\cos\left\{z\left(\rho_0-\frac{\alpha}{2}\right)+\frac{\varphi}{2}-\frac{\pi}{4}\right\}\right]\right|. \tag{30}$$

In the first maximum of breathing wave, this normalized width can be written as

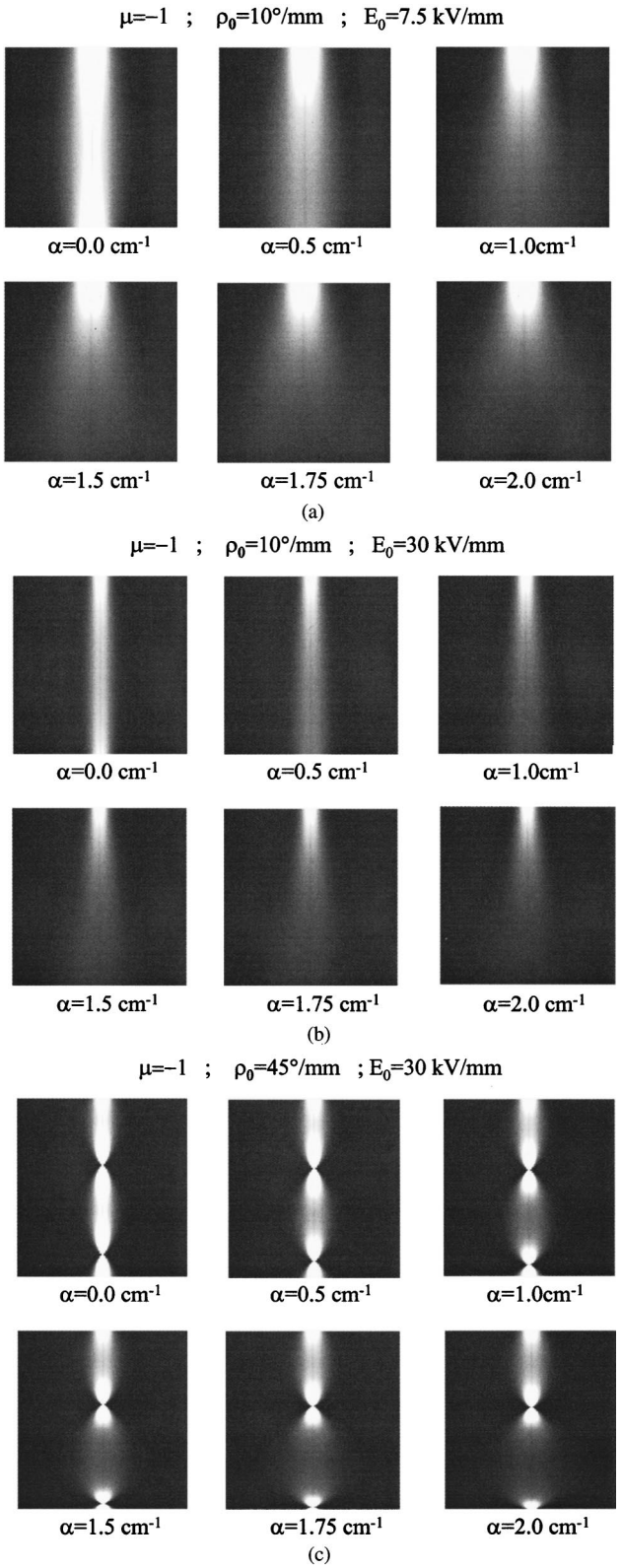

FIG. 3. The total intensity of the propagating wave as a function of the distance with the external electric field, E_0, applied along the [110] crystal direction ($\mu=-1$, perpendicular to the vertical propagation axis, Oz), for different absorption coefficients. The maximum propagation distance was taken 8 mm. (a) BTO crystal, $E_0=7.5$ kV/mm; (b) BTO crystal, $E_0=30$ kV/mm; (c) BSO crystal, $E_0=30$ kV/mm (according to the material parameters in [17]).

$$(\Delta\rho)_{1\,\max}=\sqrt{\pi/2r}\frac{2\rho_0-\alpha}{\sqrt{\alpha^2+(2\rho_0-\alpha)^2}}\times\exp\left\{\frac{\alpha}{2\rho_0-\alpha}\left[\arctan\left(\frac{\alpha}{2\rho_0-\alpha}\right)+\frac{\pi}{4}\right]\right\}=(\Delta\rho)_{1\,\max}\left(r,\frac{\alpha}{2\rho_0}\right). \tag{31}$$

The maximum soliton width can be immediately derived as

$$w_{s1}=(\Delta\rho_{1\,\max})/k\sqrt{n_0^2 r_{41}E_0}. \tag{32}$$

In the total intensity (29), the optical activity (included in γ) leads to the breathing. The total intensity decreases strongly with the propagation distance due to the large absorption (included as well in γ) and, for this reason, sillenite crystals longer than few millimeters can practically not be used. The absorption leads also to a progressive decrease of the diffraction compensation by the nonlinear birefringence (dominated by drift effect). However, for the usual sillenite crystal lengths and absorption, the soliton confinement is reasonably good. It can be noticed that the soliton intensity reaches high values in the points of the z axis defined by

$$\cos\left[z\left(\rho_0-\frac{\alpha}{2}\right)+\frac{\varphi}{2}-\frac{\pi}{4}\right]=0,$$

where a focusing occurs (within the power conservation).

One can observe that the period of the transverse modulation as well as the soliton width (in the first half-period) increase slightly with the absorption growth, for strong optical activity [Figs. 4(a,b)]. For the usual parameter values and the external field $E_0=30$ kV/cm, the breathing period could increase for BSO crystals from 0.8 cm (without absorption) to $\approx$1 cm (with $\alpha=1.7\ \mathrm{cm}^{-1}$) and for BTO crystals, from 5.7 (without absorption) to 7.3 cm (with $\alpha=0.5\ \mathrm{cm}^{-1}$) [Fig. 4(a)]. For absorption coefficient $\alpha=1.7\ \mathrm{cm}^{-1}$ and BSO crystal length of 2 mm, the soliton width increase is of the order of 17% [Fig. 4(c)]. According to Eq. (32), the optical activity would decrease the soliton width [Figs. 4(b) and 4(c)]. The soliton width increase due to absorption is compensating in a favorable manner the decrease in width in the focusing interval (at least in the first half-period of the breathing, which is, for BSO crystals, $\approx$5 mm). Thus, the beam confinement is even improved in the experiments with the usual crystals.

B. Solitonlike analytical solutions of the wave equations in PRC with optical activity and absorption for signals comparable to the background

For *signal intensity comparable with the background intensity*, the intensity dependent factor from Eq. (4) can be approximated by $\frac{1}{4}(3\text{-}I/I_B)$. Equations (14) become

$$2i\frac{\partial\Phi_{x1}}{\partial\zeta'}+\frac{\partial\Phi_{x1}}{\partial\rho^2}+(\mu/4)\left[3-r\frac{2}{\pi}\gamma^2(\varphi,\zeta')(\Phi_{x1}^2+\Phi_{y1}^2)\right]\Phi_{x1}=0,$$

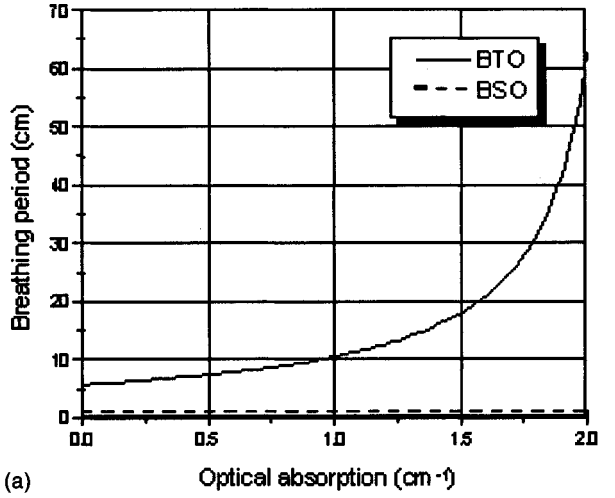

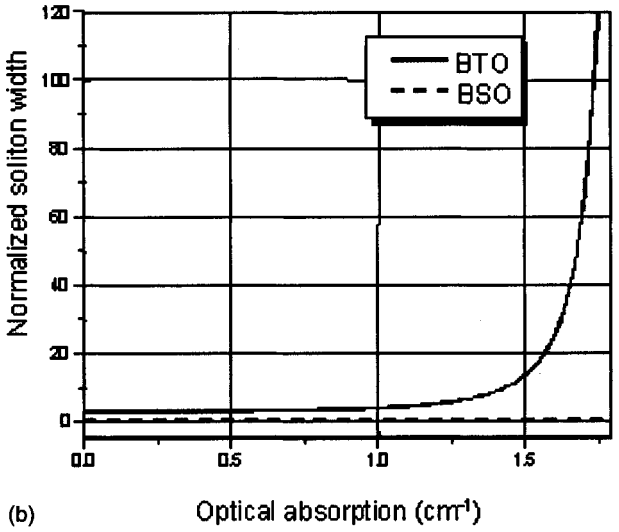

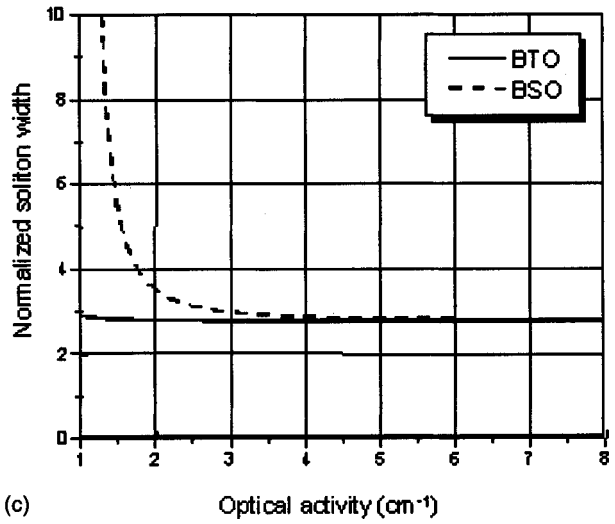

FIG. 4. The dependence of the soliton breathing period and the normalized soliton width on the absorption coefficient [(a) and (b)] and on the optical activity (c), at low intensity.

$$2i\frac{\partial\Phi_{y1}}{\partial\zeta'}+\frac{\partial\Phi_{y1}}{\partial\rho^2}+(1/4)\left[3-r\frac{2}{\pi}\gamma^2(\varphi,\zeta')(\Phi_{x1}^2+\Phi_{y1}^2)\right]\Phi_{y1}=0. \tag{33}$$

The transverse component decoupling as in Eq. (18) leads to the transverse equations system

$$\frac{\partial^2\psi_x(\rho_1)}{\partial\rho^2}-\mu(r/4)\frac{2}{\pi}\gamma^2(\varphi,\zeta')(\psi_x^2+\psi_y^2)\psi_x=0,$$

$$\frac{\partial^2\psi_y(\rho_1)}{\partial\rho^2}-(r/4)\frac{2}{\pi}\gamma^2(\varphi,\zeta')(\psi_x^2+\psi_y^2)\psi_y=0, \tag{34}$$

with

$$\rho_2=\sqrt{r/2\pi}\,\gamma(\varphi,z)\rho=\sqrt{r/2\pi}\,e^{-\alpha z/2}\left|\cos\left(\frac{1}{2}\right)\right.$$
$$\left.\times\left(\varphi+g_1kz-\frac{\pi}{2}\right)\right|^{-1}\rho=\rho/(\Delta\rho)_2. \tag{35}$$

In this case, the soliton intensity takes the same form as in the case of low intensity. The width of the solitonic channel can be defined similarly to Eq. (31),

$$(\Delta\rho)_{2,\max}=\sqrt{2\pi/r}\frac{2\rho_0-\alpha}{\sqrt{\alpha^2+(2\rho_0-\alpha)^2}}$$
$$\times\exp\left\{\frac{\alpha}{2\rho_0-\alpha}\left[\arctan\left(\frac{\alpha}{2\rho_0-\alpha}\right)+\frac{\pi}{4}\right]\right\}, \tag{36}$$

$$w_{s2}=(\Delta\rho_{2\,\max})/k\sqrt{n_0^2r_{41}E_0}, \tag{37}$$

but it is smaller due to the different range of values for r,

$$w_{s2}\approx 2\sqrt{r_1/r_2}\approx 2\sqrt{r_1}<w_{s1} \tag{38}$$

(indices 1 and 2 correspond to low and medium intensities, around 1). This result is in agreement with the experimental results. The period of the transverse modulation as well as the soliton width (in the first half-period) are increasing with the absorption growths, for strong optical activity, as in the case of low intensity.

C. Analytical solutions of the wave equations in PRC with large optical activity and absorption for high signal to background intensity ratio

In this case, the intensity dependent factor from Eq. (4) (proportional to the spatial charge field in the photorefractive crystal) can be written as

$$E_{SC}\sim\frac{1}{1+(I/I_B)}\sim\frac{1}{(I/I_B)}=\frac{I_0}{rI},\quad r=\frac{I_0}{I_B} \tag{39}$$

and the equations of the field (Φ_{x_1},Φ_{y_1}) take the form

$$2i\frac{\partial\Phi_{x_1}}{\partial\zeta'}+\frac{\partial^2\Phi_{x_1}}{\partial\rho^2}+\frac{\mu}{(2r/\pi)\gamma^2[\Phi_{x_1}^2+\Phi_{y_1}^2]}\Phi_{x_1}=0,$$

$$2i\frac{\partial\Phi_{y_1}}{\partial\zeta'}+\frac{\partial^2\Phi_{y_1}}{\partial\rho^2}+\frac{1}{(2r/\pi)\gamma^2[\Phi_{x_1}^2+\Phi_{y_1}^2]}\Phi_{y_1}=0. \tag{40}$$

Using again the decoupling of the transverse component equation system, we obtain

$$\frac{\partial^2\psi_x(\rho)}{\partial\rho^2}-\mu\frac{\psi_x}{(2r/\pi)\gamma^2(\psi_x^2+\psi_y^2)}=0,$$

$$\frac{\partial^2\psi_y(\rho)}{\partial\rho^2}-\frac{\psi_y}{(2r/\pi)\gamma^2(\psi_x^2+\psi_y^2)}=0. \tag{41}$$

We can renormalize Eqs. (41) to

$$\rho_3=\rho/(\Delta\rho)_3=\rho/(\sqrt{2r/\pi}\gamma)$$
$$\approx\left[\sqrt{\pi/2r}e^{\alpha z/2}\cos\left(\frac{1}{2}\phi+\frac{1}{2}g_1kz-\frac{\pi}{4}\right)\right]\rho.$$

Case 1. $\mu=0$. From Eqs. (40) and (41), one can obtain the solutions

$$\psi_x(\rho,\zeta')=\exp\{-[\rho_3^2w_0^2/(w_0^4+4\zeta'^2)]\}[\pi^2(w_0^4+4\zeta'^2)]^{-1/4},$$

$$\psi_y(\rho,\zeta')=\pm\frac{\sqrt{2}\psi_x}{\cosh[\rho_3-S_h^2/(1+S_h^2)]},$$

$$S_h^2=\sqrt{\pi^2/2w_0^4(w_0^4+4\zeta'^2)\psi_y(0,\zeta')-1}. \tag{42}$$

Assuming that the usual crystal length is small (to have acceptable attenuation) and that the perturbation term along the propagation axis (S_h) is negligible, the total intensity of this solitonlike wave takes the form

$$I(\rho,\varphi,\zeta')=(2/\pi)I_B(r\gamma^2)[\psi_x^2+\psi_y^2]\approx(2/\pi^2w_0^2)I_B(r\gamma^2)\times\exp(-2\rho_3^2/w_0^2)[1+2\cosh^{-2}(\sqrt{2}\rho_3)]. \tag{43}$$

The total intensity from Eq. (43) is apparently similar to that obtained at low intensity. However, the dependence of ρ_3 on the axial function γ is inverted in this situation. One can remark that the solitonlike propagation is maintained here in the presence of optical activity and absorption, with better confinement at higher external electric fields. The increase of optical activity (at given absorption coefficient) decreases the soliton breathing period and the increase of absorption coefficient (at a given optical activity) slightly increases the soliton breathing period, with a simultaneous attenuation increase and soliton width decrease.

We can remark that, at the propagation distances for which $\gamma\to\infty$, the solution (42) cannot hold and the y component should be replaced as well by the linear diffraction solution derived directly from Eqs. (40) leading to

$$I(\rho,\varphi,\zeta')\approx2\exp\{-[2\rho^2w_0^2/(w_0^4+4\zeta'^2)]\}\times[\pi^2(w_0^4+4\zeta'^2)]^{-1/2}. \tag{44}$$

Thus, in these points, the wave intensity loses the confinement and tends to the linear diffracting limit, with its width growing up to the normal diffracted beam width,

$$\Delta\rho=w_0\sqrt{1+4\zeta'^2/w_0^4}. \tag{45}$$

This periodic behavior cannot disturb too much the solitonic confinement in the most part of the propagation process.

The soliton width is obtained by combining the width of the hyperbolic secant (which is close to a corresponding Gaussian function), for cos function equal to 1,

$$(\Delta\rho)_{3s}=\sqrt{r/2\pi}\gamma=\sqrt{r/2\pi}e^{-\alpha z/2}, \tag{46a}$$

and the width of the Gaussian function of Eq. (43). Thus, we can calculate the maximum soliton width by

$$(\Delta\rho_t)^{-2}\approx(\Delta\rho_{3s})^{-2}+(w_0\gamma\sqrt{r/\pi})^{-2}=(2\pi/r\gamma^2)[1+(\sqrt{2}w_0)^{-2}]. \tag{46b}$$

We can observe that the soliton width is smaller than the Gaussian input beam (as expected) and increases also with the increase of the beam ratio, r. As all transverse variables were normalized, one can obtain the actual soliton width, $w_{s\,\max}=(\Delta\rho_t)/k\sqrt{n_0^2r_{41}E_0}$ and deduce its dependence on the external electric field. The initial conditions lead to the relation $w_0\approx6r/\pi^{3/2}$ and to small w_0, which introduce restrictive conditions for $(2+1)$D solitons, which were observed in experiments with other materials.

Case 2. $\mu=-1$. One can derive as for the low intensity case,

$$\frac{\partial^2\psi_x(\rho_3)}{\partial\rho_3^2}+\frac{\psi_x}{\psi_x^2+\psi_y^2}=0,$$

$$\frac{\partial^2\psi_y(\rho_3)}{\partial\rho_3^2}-\frac{\psi_y}{\psi_x^2+\psi_y^2}=0. \tag{47}$$

The solutions of the equation system (47) can be written in the matrix form

$$\begin{bmatrix}\psi_x(\rho_3)\\ \psi_y(\rho_3)\end{bmatrix}=e^{-S_1(\rho_3)}\begin{bmatrix}\cos S_2(\rho_3) & \sin S_2(\rho_3)\\ -\sin S_2(\rho_3) & \cos S_2(\rho_3)\end{bmatrix}\begin{bmatrix}\psi_x(0)\\ \psi_y(0)\end{bmatrix}, \tag{48}$$

where

$$S_1(\rho_3)=\left|\frac{1-\cosh^2 2\beta+\sin^2 2\alpha}{(\cosh 2\beta+\cos 2\alpha)^2}\right|,$$

$$S_2(\rho_3)=\left|\frac{2\sin 2\alpha\sinh 2\beta}{(\cosh 2\beta+\cos 2\alpha)^2}\right|,$$

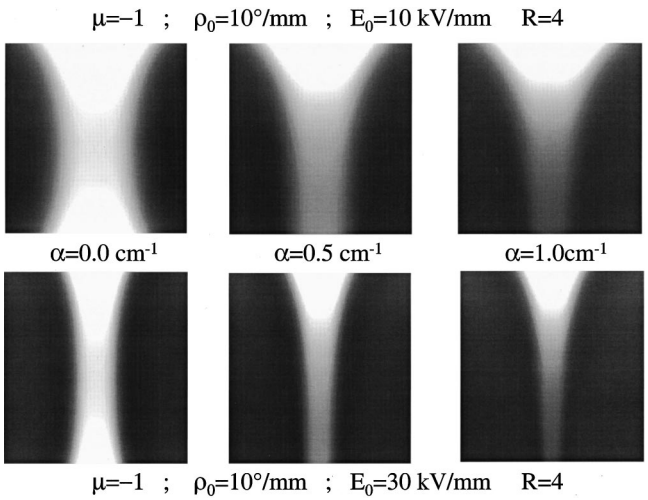

FIG. 5. The total intensity of the propagating wave as a function of the distance in a BTO crystal, at high intensity ratio, $r=4$, with the external electric field, E_0, applied along the [110] direction and perpendicular to the vertical propagation axis, Oz, for different absorption coefficients, α. The maximum propagation distance was taken 8 mm.

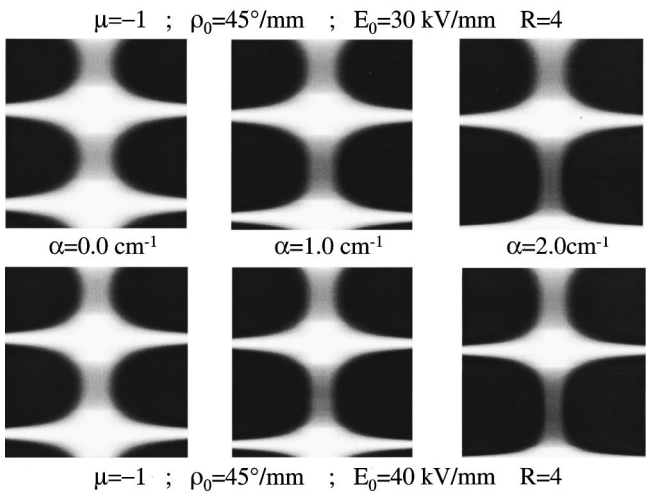

FIG. 6. The total intensity of the propagating wave as a function of the distance in a BSO crystal, at high intensity ratio, $r=4$, with the external electric field, E_0, applied along the [110] direction and perpendicular to the vertical propagation axis, Oz, for different absorption coefficients, α. The maximum propagation distance was taken 8 mm. The wave intensity profile, around the points with $\gamma \rightarrow \infty$, is oversized by Eq. (51), instead of enlarging up to the normal diffraction width.

and

$$\alpha = \sqrt{\pi/2}\frac{\psi_x(0)}{\psi_x^2(0)+\psi_y^2(0)}\rho_3,$$

$$\beta = -\sqrt{\pi/2}\frac{\psi_y(0)}{\psi_x^2(0)+\psi_y^2(0)}\rho_3. \tag{49}$$

The optical field components can be written as

$$\begin{bmatrix} A_x(\rho_3,\varsigma') \\ A_y(\rho_3,\varsigma') \end{bmatrix} = \sqrt{2I_B r/\pi}\,\gamma(\varphi,\varsigma')e^{-S_1(\rho_3)}\begin{bmatrix} \sin\theta & -\cos\theta \\ \cos\theta & \sin\theta \end{bmatrix} \times \begin{bmatrix} e^{-i\varsigma'/2}\cos S_2(\rho_3) & e^{-i\varsigma'/2}\sin S_2(\rho_3) \\ -e^{i\varsigma'/2}\sin S_2(\rho_3) & e^{i\varsigma'/2}\cos S_2(\rho_3) \end{bmatrix} \times \begin{bmatrix} \psi_x(0) \\ \psi_y(0) \end{bmatrix}. \tag{50}$$

Equation (50) allows us to calculate the $(2+1)$D wave intensity. If we consider the initial conditions $\psi_x(0)=\psi_y(0)=\psi_0=(\sqrt{\pi}/4w_0)^{1/2}$, then

$$\alpha = -\beta = \sqrt{\pi/2}\frac{\rho_3}{2\psi_0} = \frac{\pi}{4}\frac{\rho}{\psi_0\gamma\sqrt{r}} = (\pi/4)^{1/4}\frac{\rho}{\gamma\sqrt{rw_0}},$$

$$I_S(\rho_3,z) = \frac{1}{\sqrt{\pi}}I_B\frac{r\gamma^2(\varphi,z)}{w_0}e^{-2S_1(\rho_3)}, \tag{51}$$

which is a breathing wave with the same period as in the previous cases (Fig. 5, for BTO crystals and Fig. 6, for BSO crystals).

We can remark that at the propagation distances, for which $\gamma \rightarrow \infty$, this solution cannot hold and it should be replaced by the solution of the linear system (diffraction) derived directly from Eqs. (40), as for Eqs. (44). In these points, the beam intensity width tends to the linear diffracting limit, i.e., the channel width is growing up to $\Delta\rho = w_0\sqrt{1+4\zeta'^2/w_0^4}$. This periodic behavior does not disturb too much the solitonic confinement in the most part of the propagation process (Figs. 5 and 6). Actually, in Fig. 6, the solution of linear diffraction is not introduced and the local deformations of the solitonlike wave (in the vicinity of the distances at which $\gamma \rightarrow \infty$) are exaggerated by the solution (51).

The normalized widths of the wave component envelopes are

$$\rho_{3x} = 2\alpha = \frac{\rho}{\Delta\rho_{3x}}, \quad \rho_{3y} \equiv -2\beta = -\frac{\rho}{\Delta\rho_{3y}},$$

$$\Delta\rho_{3x} = |\Delta\rho_{3y}| = (4/\pi)^{1/4}\gamma\sqrt{rw_0}. \tag{52}$$

The proportionality of the wave widths to $\sqrt{r}$ corresponds to the experimental findings. The initial conditions introduce additional constraints, r higher than but close to 1 and $w_0^3 = r/\pi^{3/2}$, which are important in the experimental observation of these solitonlike waves.

If we consider the $(1+1)$D case: $\psi_x(0)=0$; $\psi_y(0)=1$, one can find

$$2\alpha = 0, \quad S_2(\rho_3) = 0, \quad S_1(\rho_3) = th^2\rho_{3y}$$

and

$$I_S(\rho_{3y},\zeta') \cong \frac{2}{\pi}I_B r\gamma^2(\varphi,\zeta')\frac{1}{\cosh^2(\rho/\Delta\rho_{3y})},$$

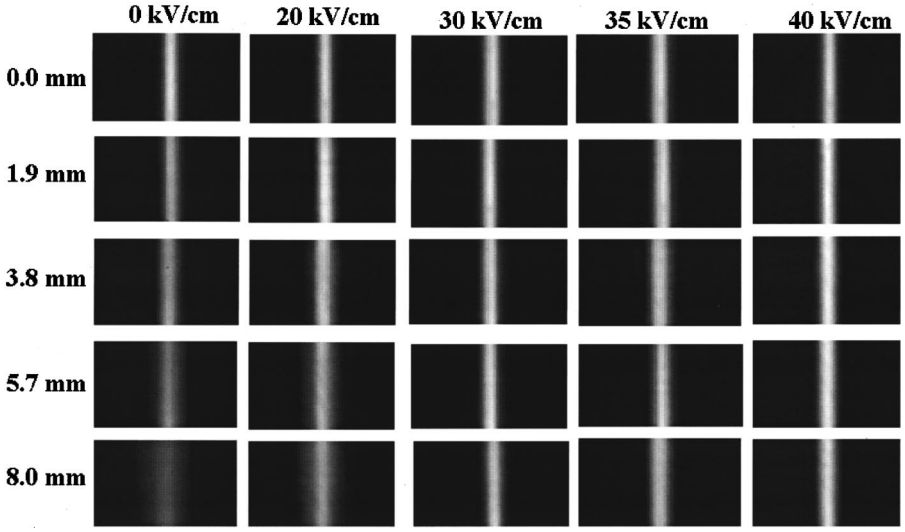

FIG. 7. The experimental images of signal wave propagation and soliton formation, in a BSO crystal, for different external electric fields (displayed horizontally) and propagation distances (shown vertically).

$$\Delta\rho_{3y}=\frac{\gamma\sqrt{r}}{\pi}, \quad \Delta\rho_{3x}\to\infty. \tag{53}$$

III. EXPERIMENTAL AND NUMERICAL VERIFICATION OF THE ANALYTICAL SOLUTIONS OF SOLITONLIKE WAVES IN BSO CRYSTALS

Solitonic propagation of laser beams inside photorefractive BSO crystals has been experimentally demonstrated using the setup shown in Fig. 1. The BSO crystal was 8 mm long and was biased by a static electric field along its [001] crystallographic direction [which corresponds to $\mu=0$ condition in Eq. (7)]. It is simultaneously illuminated by the focused Gaussian signal beam and by the uniform background beam (I_B), at $\lambda=514$ nm. In order to avoid electric discharge in air due to the high static electric fields (up to 40 kV/cm), the crystal is kept in an insulating liquid cell. A laser beam, orthogonally polarized with respect to the background, is focused with a cylindrical lens on the crystal, giving a $(1+1)$D light beam (a light "sheet" with thickness of 15 μm), at the input. The background is copropagated inside the crystal with a small angle with respect to the signal beam in order to obtain, far from the crystal, two well-separated beams, from which the signal beam can be extracted by hard filtering.

Using this procedure, any coherent interaction between soliton and background beams, which might come out from any modification of the beam polarization, is strongly reduced. This configuration is preferable to the side-illumination one also for the reason that the copropagating beams suffer the same absorption and their intensity ratio, $r=I_0/I_B$, remains constant. After the crystal, a focusing lens images the output signal beam on a charge coupled device camera with a magnification factor of about 20.

The complete recording of propagation and soliton formation is presented in Fig. 7, where the experimental images for different external electric fields and propagation distances are shown. At 0 kV/cm, as well as at 20 kV/cm, the signal beam is enlarged by diffraction; for the second bias, a self-focusing is present, which leads to a smaller beam width than in the former case (at 8 mm propagation distance). The soliton is instead formed only at electric fields equal or higher than 30 kV/cm, for which the signal beam keeps the same width along the entire propagation distance. At electrical fields higher than 35 kV/cm, the soliton breathing becomes evident (Fig. 8), as described analytically and numerically.

In Fig. 9, the normalized experimental beam waists are shown versus the signal/background intensity ratio, r, at $E_0=40$ kV/cm, together with the analytical solutions (solid lines) and with numerical solutions of Eq. (3) (dashed line). It is interesting to note that the normalized waists scale as $(I_0/I_B)^{-1/2}$ for low I_0/I_B (in this case <1), while they scale

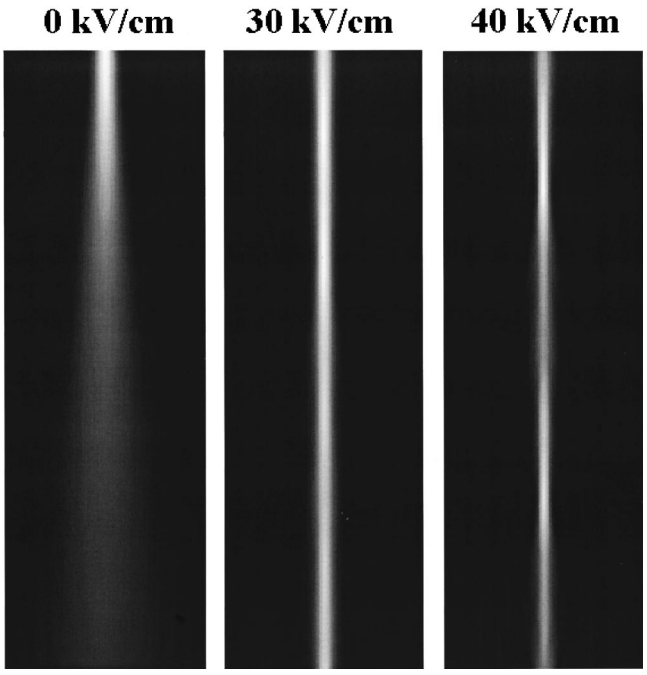

FIG. 8. The simulation of signal wave propagation in a BSO crystal, for different external electric fields (displayed horizontally) and large propagation distance (six diffraction lengths), which show the soliton formation and the breathing occurrence (at 30 and 40 kV/cm).

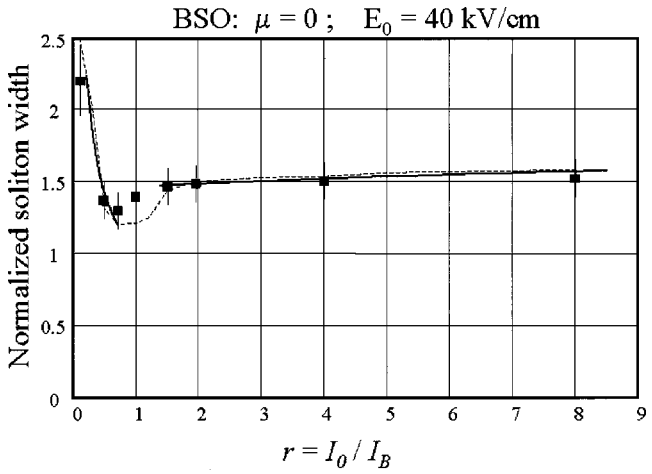

FIG. 9. The normalized experimental beam waist versus the signal/background intensity ratio, r, at $E_0 = 40$ kV/cm, together with the analytical solutions (solid lines) and with numerical solutions of Eq. (3) (dashed line). The normalized waists scale as $(I_0/I_B)^{-1/2}$ for low I_0/I_B (in this case <1), while they scale as $0.06(I_0/I_B)^{1/2}+\text{bias}$, for high I_0/I_B (>2).

s $0.06(I_0/I_B)^{1/2}+\text{bias}$ for high I_0/I_B (>2). The numerical simulations derive from the use of a BPM code, which was described in [22]. For the same external electric field, both the numerical integration and the experimental data show a minimum $(1+1)$D soliton width at $r \approx 0.8$, which cannot be predicted by the analytical solutions. The experimental data show that the breathing period is not constant, but depends on the experimental conditions, as it was analytically described. The agreement between the analytical, numerical, and experimental data is good.

IV. CONCLUDING REMARKS

We have obtained analytical solutions for the light propagation in the most complex optical photorefractive materials, involving induced optical birefringence, optical activity, and absorption. In cubic PRC, we have demonstrated the occurrence of $(2+1)$D spatial solitonlike waves, for the external electric field applied along [001] and [110] crystal axes. The spatial solitons are transversely modulated (breathing), due to the combined action of the optical activity and absorption. The components of the rotatory optical field are coupled and interchange energy in the wave propagation along z axis. The polarization of the incident field is changed in the propagation.

The conditions for the occurrence of $(2+1)$D solitons are more complex than in the case of $(1+1)$D solitons and lead to a more limited range of experimental parameters $(w_0, E_0, r = I_0/I_B)$.

The analytical results are supported by our numerical simulations and experimental results, which were obtained with BSC photorefractive crystals exhibiting large optical rotating power and absorption. The solitonic behavior and the soliton breathing at high external electric fields, as well as the soliton width dependence on the beam intensity ratio, show a good agreement between the theoretical and experimental data. Our results are in agreement with the numerical ones obtained by Krolikowski *et al.* [19], in the $(1+1)$D case, without absorption.

The theoretical derivation of the dependence of the soliton features on different controllable parameters is done in order to further exploit our solutions. The breathing period increases with the absorption growth, for strong optical activity. The soliton width (in the first half-period, which matches the usual crystal lengths) decreases with the beam ratio, r, at low intensity and increases with r, at high intensity. The dependence of soliton width on absorption coefficient is inverted with respect to that on r.

ACKNOWLEDGMENTS

V.V. acknowledges the support of The ''Abdus Salam'' International Center for Theoretical Physics, Trieste, Italy and the support of Professor Giuseppe Furlan, for the TRIL 5512.NI.H8 and A7 Grants, which made possible this common work at Universita degli Studi di Roma ''La Sapienza.'' A COST P2 project of the European Union was also very useful for this collaborative research.

[1] M. Segev, G. C. Valley, B. Crosignani, P. di Porto, and A. Yariv, Phys. Rev. Lett. **73**, 3211 (1994).
[2] M. Segev, M. Shih, and G. C. Valley, J. Opt. Soc. Am. B **13**, 706 (1996).
[3] D. N. Christodoulides and M. I. Carvalho, J. Opt. Soc. Am. B **12**, 1628 (1995); Opt. Lett. **19**, 1714 (1994).
[4] B. Crosignani, M. Segev, D. Engin, P. di Porto, A. Yariv, and G. J. Salamo, J. Opt. Soc. Am. B **10**, 446 (1993).
[5] B. Crosignani, P. di Porto, A. Degasperis, M. Segev, and S. Trillo, J. Opt. Soc. Am. B **14**, 3078 (1997).
[6] M. Shih, M. Segev, G. C. Valley, G. Salamo, B. Crosignani, and P. di Porto, Electron. Lett. **31**, 826 (1995).
[7] M. D. Iturbe Castillo, P. A. Marquez Aguilar, J. J. Sanchez Mondragon, S. Stepanov, and V. Vysloukh, Appl. Phys. Lett. **64**, 408 (1994).
[8] M. D. Iturbe Castillo, J. J. Sanchez Mondragon, S. Stepanov, M. B. Klein, and B. A. Wechsler, Opt. Commun. **118**, 515 (1995).
[9] M. Shih, P. Leach, M. Segev, M. H. Garrett, G. Salamo, and G. C. Valley, Opt. Lett. **21**, 324 (1996).
[10] K. Kos, H. Meng, G. Salamo, M. Shih, M. Segev, and G. C. Valley, Phys. Rev. E **53**, R4330 (1996).
[11] Z. Chen, M. Mitchell, M. Shih, M. Segev, M. H. Garrett, and G. C. Valley, Opt. Lett. **21**, 629 (1996).
[12] N. Fressengeas, D. Wolfensberger, J. Maufoy, and G. Kugel, J. Appl. Phys. **85**, 2062 (1999).
[13] D. Wolfensberger, N. Fressengeas, J. Maufoy, and G. Kugel, J. Appl. Phys. **89**, 2511 (2001).
[14] M. Segev, B. Crosignani, G. J. Salamo, G. C. Duree, Jr., P. di Porto, and A. Yariv, in *Photorefractive Effects and Materials*, edited by D. D. Nolte, (Kluwer Academic, Boston, 1995), p. 221.

[15] B. Crosignani, P. di Porto, M. Segev, G. J. Salamo, and A. Yariv, Riv. del Nuovo Cimento **21**, 1 (1998).
[16] C. Denz, J. Petter, C. Weilnau, and M. Ahles, CLEO/Europe-EQEC Digest, Munich, 2001 (unpublished), p. 163
[17] M. P. Petrov, S. I. Stepanov, and A. V. Khomenko, *Photorefractive Crystals in Coherent Optical Systems* (Springer, Berlin, 1991).
[18] S. R. Singh and D. N. Christodoulidis, J. Opt. Soc. Am. B **13**, 719 (1996).
[19] W. Krolikowski, N. Akhmediev, D. R. Andersen, and B. Luther-Davies, Opt. Commun. **132**, 179 (1996).
[20] V. I. Vlad, V. Babin, M. Bertolotti, E. Fazio, and M. Zitelli, Programme of OSA Annual Meeting, Santa Clara, 1998, Paper ThCC7 (unpublished), p. 143; Proc. Romanian Academy **A1**, 25 (2000).
[21] E. Fazio, F. Mariani, A. Funto, M. Zitelli, M. Bertolotti, V. Babin, and V. I. Vlad, Proc. SPIE **4430**, 411 (2001); J. Opt. **A3**, 466 (2001).
[22] J. P. Herriau, D. Rojas, J. P. Huignard, J. M. Bassat, and J. C. Launay, Ferroelectrics **66**, 1 (1986).
[23] S. Blair, K. Wagner, and R. McLeod, J. Opt. Soc. Am. B **13**, 2141 (1996).
[24] V. I. Vlad, V. Babin, M. Bertolotti, and E. Fazio, Proc. SPIE **4430**, 418 (2001).